Environmental Science and Pollution Research (2023) 30:95493–95506
https://doi.org/10.1007/s11356-023-29082-8

RESEARCH ARTICLE

Enhanced arsenite removal in aqueous with Fe-Ce-Cu ternary oxide nanoparticle

Ying Liu[1] · Leyi Li[1] · Xuemei Huang[1] · Yaochi Liu[1]

Received: 6 January 2023 / Accepted: 27 July 2023 / Published online: 8 August 2023

Abstract

Arsenite is both more harmful and challenging to get out of water than arsenate. For enhanced As (III) removal, a ternary oxide nanoparticle (FCCTO) mainly composed of iron(Fe), with a small proportion of cerium(Ce) and copper(Cu) was created using a coprecipitation–calcination process. FCCTO was found to be effective in removing As (III) from water, with factors such as adsorbent dose, pH, temperature, and coexisting anions influencing its efficiency. The surface area of FCCTO reached 180.2 m^2/g and the doping significantly increased its pore volume and diameter. The adsorption process on FCCTO was endothermic and spontaneous. Ce and Cu in FCCTO were able to efficiently oxidize 81.3% As (III) to As(V). Abundant sites were provided by surface hydroxyl groups for arsenic adsorption. The maximal As(III) adsorption capacity of this adsorbent under the synergistic impact of oxidation and adsorption was 101.5 mg/g. After five cycles, the FCCTO's As(III) adsorption rate dropped to 60% as a result of tetravalent Ce consumption. Surface complexation, redox, and adsorption all had a significant impact on the adsorption process. Overall, FCCTO was an excellent adsorbent with benefits of being facile fabrication, environmentally, recyclable, and having a high As(III) adsorption capacity.

Keywords Fe-Ce-Cu ternary oxide · Arsenite · Adsorption · Oxidation · Mechanism

Introduction

Arsenic (As) contamination mainly caused by geologic arsenic cycling and anthropogenic activities including pesticide applications, mining, and geothermal energy, and is critical concerned due to its carcinogenicity and high harmfulness (Masuda 2018). Trivalent As(III) and pentavalent As(V) are the two primary types of arsenic that are present in the environment (Ayub et al. 2022). As(III) is more prevalent in waterbodies than As(V) and is more hazardous because of its high mobility. The maximum allowed level of arsenic in drinking water has been set by the World Health Organization (WHO) as 10μg L^{-1} (WHO 2010).

Arsenic can be removed from water using a variety of technologies, including coagulation sedimentation (Lin et al. 2015), ion exchange (Koseoglu et al. 2011), adsorption (Sherlala et al. 2019; Ayub et al. 2020), membrane separation (Çermikli et al. 2020), electrolysis (Nanseu-Njiki et al. 2007), and biochemical methods (Song et al. 2014). Sorption is a high efficiency, simple, and convenient arsenic treatment method. Metal oxide–based adsorbents had extensively employed to extract arsenic from water owing to the large number of surface functional groups (Gupta et al. 2021; Luo et al. 2012; Yoon et al. 2016; Luo et al. 2013), but arsenite is difficult to attach onto metal oxide through electrostatic interaction and its removal commonly needs oxidation pretreatment by chlorine (Sorlini and Gialdini 2010), hydrogen peroxide (Shan et al. 2022), or ozone (Kim and Nriagu 2000). Adding oxidants (Dodd et al. 2006) or assisting photocatalytic oxidation (Zhang et al. 2018) can realize the high efficiency removal of As(III); however, the process becomes complex. It is significant to develop materials with both adsorption and As(III) oxidation.

Metal oxide, especially iron (hydr)oxide and its modified materials, are environmentally friendly adsorbents and have significant affinity and good stability for arsenic. The commercialized granulated ferric hydroxide (GFH) (Zhang et al. 2010) has been used for As(III) removal under auxiliary oxidation (Siddiqui and Chaudhry 2017). Binary or ternary

Responsible Editor: Ioannis A. Katsoyiannis

✉ Yaochi Liu
liuyaochi72@163.com

[1] College of Chemistry and Chemical Engineering, Central South University, Changsha 410083, China

oxides with dual effects of oxidation and adsorption (Han et al. 2022) have also been applied to arsenic removal, such as Fe-Mn (Zhang et al. 2007), Ce-Mn (Chen et al. 2018), Fe-Cu binary oxide (Wang et al. 2022), and Fe-Mn-Cu ternary oxide (Wu et al. 2021). Multi oxides containing manganese oxide has excellent arsenic oxidation performance, but it may lead to manganese pollution in acidic environments (Li et al. 2012; Yin et al. 2020). The investigation about Fe-Mn-Cu ternary oxide found that the addition of copper activated the redox effect of manganese oxide and greatly improved the removal performance. Copper oxides can exert fine oxygen exchange performance through the oxidation–reduction cycle of Cu(II)/Cu(I) (Huang et al. 2018).

Optimizing the mixture of multi-component oxides is required to provide an affordable, ecologically friendly adsorbent. Cerium oxide–containing adsorbents have strong catalytic oxidation performance and specific affinity with arsenic (Li et al. 2021; Hoang et al. 2022). Ceria anchored on carbon nanotubes (Peng et al. 2005), cerium oxide nanoparticles loaded into silicon (Sun et al. 2012), and CeO_2–ZrO_2 nanospheres (Xu et al. 2013) showed excellent As(V) adsorption performance. Chitosan treated with cerium displayed performance for rapid oxidation and As(III) adsorption (Zhang et al. 2016). Fe-Ce oxide adsorbent (Fe/Ce=1:1.1) demonstrated significant As(V) and As(III) adsorption capacities (Zhang et al. 2003; Basu et al. 2013). The combination of copper and cerium oxides also showed high catalytic oxidation performance (Moretti et al. 2015). It is possible to predict that Fe-Ce-Cu ternary oxide will remove As(III) more effectively than Fe-Mn-Cu ternary oxide. At the same time, the problem of manganese leakage in the adsorbent containing manganese oxides is avoided.

Thus, a Fe-Ce-Cu ternary oxide (FCCTO) nanoparticle mainly composed of iron oxides was prepared by doping a small proportion of cerium and copper. Batch adsorption studies were used to examine the impacts of the adsorbent dose, initial pH value, reaction time, initial concentration, and adsorption temperature on the adsorption capacities of FCCTO. The mechanism of interaction between As(III) and FCCTO was discussed through the study of adsorption kinetics, isotherm, and thermodynamics.

Material and methods

Material and chemicals

Chemical reagents, such as $Fe(NO_3)_3{\cdot}7H_2O$ and $NaAsO_2$, were acquired from Sinopharm Chemical Reagent Co. $Ce(NO_3)_3{\cdot}6H_2O$ and NaOH were purchased in Macklin, and $CuSO_4{\cdot}5H_2O$ was purchased from Kermel Chemical Reagent Co. Ltd. (Tianjin, China), all of which were analytical grade. Purified deionized water was used during the solution preparation and equipment cleaning process. In order to make As(III) stock solution, $NaAsO_2$ was dissolved in Milli-Q water. The necessary concentration was freshly attained by fractionally dilution with deionized water.

Preparation of adsorbents

Fe-Ce-Cu ternary oxide (FCCTO) was fabricated via coprecipitation–calcination process. 0.3mol/L $Fe(NO_3)_3{\cdot}7H_2O$, 0.08mol/L $Ce(NO_3)_3{\cdot}6H_2O$, and 0.05mol/L $CuSO_4{\cdot}5H_2O$ were dissolved in distilled water respectively, then mixed them slowly in one breaker. The combined solution was heated in a water bath at 40°C during 30 min of stirring. A 0.1mol/L NaOH solution was employed to raise pH of the solution to 11, then stirred for 2h. After aged for 12 h, the precipitate was subsequently washed with Milli-Q water and finally vacuum dried at 353 K overnight. After being calcined in air at 473 K for 2 h, the obtained Fe-Ce-Cu ternary oxide was stored in desiccators for use. According to the above preparation process, Fe oxide (FO) and Fe-Ce binary oxide (FCBO) were prepared without Ce-Cu and Cu, respectively.

Characterization methods

The microscopic structures of adsorbents were measured using scanning electron microscopy measurement (FEG 250, FEI-Quanta, USA). A multilayer surface area and porosity analyzer (ASAP2460, USA) employing the BET technique was utilized to determine the particular surface area and pore characteristics of the adsorbents. The KBr disk method was used on a Fourier transform infrared spectrometer (Nicolet iS20, USA) to record the surface functional groups of FCCTO. X-ray photoelectron spectroscopy (XPS) studies performed utilizing XPS microprobe (K-Alpha, Thermo Scientific, USA) to investigate the surface chemistry. XRD pattern observed by an X-ray diffractometer (Ultima IV, Japan) with Cu (Kα) radiation.

Adsorption and desorption experiments

A fixed weight of adsorbent (16mg) was used in 50-mL Erlenmeyer flasks for batch adsorption tests. The flasks were shaken at the design temperature (298K) for 12 h at a shaking speed of 150 rpm in a thermostatic shaker (SHZ-82, China), after which the supernatant was put through a 0.45-μm membrane filter. An inductively coupled plasma atomic emission spectroscopy (ICP-OES) was used to determine the portion of As(III) in the filtered solution.

The effects of different FCCTO dosages (0.1 to 1.5 g/L) on the adsorption capability and removal efficiency of As(III) were investigated to obtain the optimum dosage. By adjusting pH from 3.0 to 11.0, the effects of pH on removal

capacity were examined. The 0.1 mol/L HCl and 0.1 mol/L NaOH solutions were added to the starting solution until the set pH value was achieved. A batch adsorption experiment examining the effects of temperature was adjusted to 298, 308, and 318 K. The adsorption kinetics were investigated by varying the contact time and measuring the solution concentration at intervals. The intervals for measurement were set at 5, 10, 30, 60, and 120 min.

With concentration values varying from 0.1 to 10 mmol/L, the impacts of coexisting anions (SO_4^{2-}, Cl^-, CO_3^{2-}, PO_4^{3-}, and SiO_3^{2-}) on As(III) sorption were also investigated. Five sequential cycles of sorption and desorption experiments were conducted to synthesized FCCTO's reusability. For the sorption test, 40 mL of 20 mg/L As(III) solution was added to a 50-mL conical flask with 16 mg of FCCTO. After shaken at 298 K, 150 r/min for 12 h, the adsorbents were collected, washed, and dried. For the desorption test, 0.5 mol/L NaOH solution was used as desorption agent. The adsorbed oxide was added to 40 mL NaOH solution and shaken at 298 K for 12 h. Determined the As(III) concentration and collected the regenerated oxide, washed with deionized water, and dried overnight in a vacuum drying oven at 353 K.

According to the following equation, the removal efficiency $E\%$ and adsorption capacity Q_e (mg/g) of As(III) on FCCTO were obtained:

$$E\% = \frac{(Co - Ce)}{Co} \times 100\% \tag{1}$$

$$Q_e = \frac{(Co - Ce) \times \mathrm{V}}{m} \tag{2}$$

where C_o and C_e are the As(III) starting and the equilibrium concentrations (mg/L), respectively. m is the adsorbent's weight (g) and V is the volume of solution (L).

Adsorption modeling

The pseudo-first order and pseudo-second order model equations were expressed as follows:

$$\ln\left(Q_e - Q_t\right) = \ln Q_e - k_1 t \tag{3}$$

$$\frac{t}{Q_t} = \frac{1}{k_2 {Q_e}^2} + \frac{1}{Q_e} t \tag{4}$$

where Q_e and Q_t (mg/g) are the adsorption capacities of As(III) adsorbed onto FCCTO at equilibrium and time t; k_1 (1/min) and k_2 (g/(mg min)) are the pseudo-first-order and pseudo-second-order rate constants, respectively.

The Weber and Morris theory–based intra-particle diffusion model (Eq. 5) was applied to evaluate the rate-controlling stage of the adsorption course (Chen et al. 2016).

$$Q_t = k_{\mathrm{pi}} t^{1/2} + C_i \tag{5}$$

where k_{pi} is the rate constant of stage i and C_i is the constant derived from the intercept.

The Langmuir, Freundlich, Tempkin, and D-R kinetic models equations were expressed as follows:

$$\text{Langmuir model}: \frac{C_e}{Q_e} = \frac{1}{bQ_m} + \frac{C_e}{Q_m} \tag{6}$$

$$\text{Freundlich model}: \ln Q_e = \ln K_f + \frac{1}{n} \ln C_e \tag{7}$$

$$\text{Tempkin model}: Q_e = B_T \ln A_T + B_T \ln C_e \tag{8}$$

$$\mathrm{D-R\ model}: \ln Q_e = \ln Q_s - K_e \xi^2 \tag{9}$$

$$\xi = \mathrm{R}T \ln\left[1 + \frac{1}{C_e}\right] \tag{10}$$

$$E = \frac{1}{\left(2K_e\right)^{0.5}} \tag{11}$$

where Q_e (mg/g) and Q_m (mg/g) are the saturation and maximal quantities of As(III) adsorbed. C_e (mg/L) is the equilibrium content in solution samples. The K_f (mg/g(L/mg)$^{1/n}$) and n are the Freundlich constants and b (L/mg) represents the Langmuir constants. AT (L/ mg) is the maximal binding energy constant. BT is equal to RT divided by bT, where bT (J/mol) is the Tempkin constant linked to the adsorbed heat. Qs (mg/g) and ζ represent the saturation removal capability and the Polanyi potential. Temperature and the universal gas constant abbreviated T (K) and R (8.314J/mol·K), respectively. The D-R constant, Ke (mol^2/KJ^2), allows us to compute the average adsorption energy E (kJ/mol).

Adsorption related parameters

The dimensionless separation constant R_L is usually employed to estimate the favorable degree of removal process, which could be obtained by the following equation:

$$R_L = \frac{1}{1 + bC_0} \tag{12}$$

where C_0 (mg/ L) is the initial concentration of As(III) and b (L /mg) is the Langmuir model constant.

The following equation is utilized to compute the thermodynamic parameters, including standard free energy

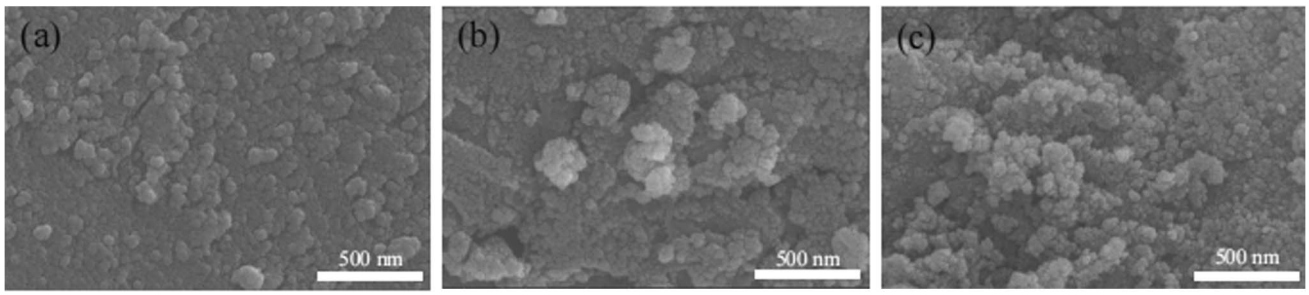

Fig. 1 SEM images of (**a**) FO; (**b**) FCBO; (**c**) FCCTO

Table 1 Porous structure parameters of FO, FCBO and FCCTO

Samples	S_{BET} (m^2/g)	V_T (cm^3/g)	D_p (nm)
FO	180.0	0.198	4.360
FCBO	178.2	0.246	5.399
FCCTO	180.2	0.445	9.726

change (ΔG^0), standard enthalpy change (ΔH^0), and standard entropy change (ΔS^0).

$$K_d = \frac{Q_e}{C_e} \tag{13}$$

$$\ln K_d = \frac{\Delta S^0}{\mathrm{R}} - \frac{\Delta H^0}{\mathrm{R}T} \tag{14}$$

$$\Delta G^0 = \Delta H^0 - T\Delta S^0 \tag{15}$$

where K_d is the distribution coefficient and R (8.314 J/mol·K) is the universal gas constant.

Results and discussion

Characteristics of adsorbents

The surface appearance of FO, FCBO, and FCCTO were investigated by SEM (Fig. 1). All three metal oxides are composed of lots of agglomerated nanoparticles. Compared with pure Fe oxide FO, the doping of Ce and Cu significantly improved the fineness of nanoparticles, which were further proved by BET data (Table 1). The BET surface areas of three adsorbents are all around 180m^2/g, but the pore volume and diameter of doping adsorbents are significantly improved. Large pore size and pore volume can speed up the mass transfer process and lower the diffusion resistance of contaminants, resulting in a rapid uptake of pollutants by materials (Wen et al. 2020).

The nitrogen adsorption–desorption isotherms of FO, FCBO, and FCCTO are depicted in Fig. 2 a–c, respectively. All three materials exhibit type IV adsorption isotherms, and the saturated adsorption plateaus on the isotherms indicate relatively uniform pore size distributions of the materials. The H_2(a) type hysteresis loops observed in FO and FCBO

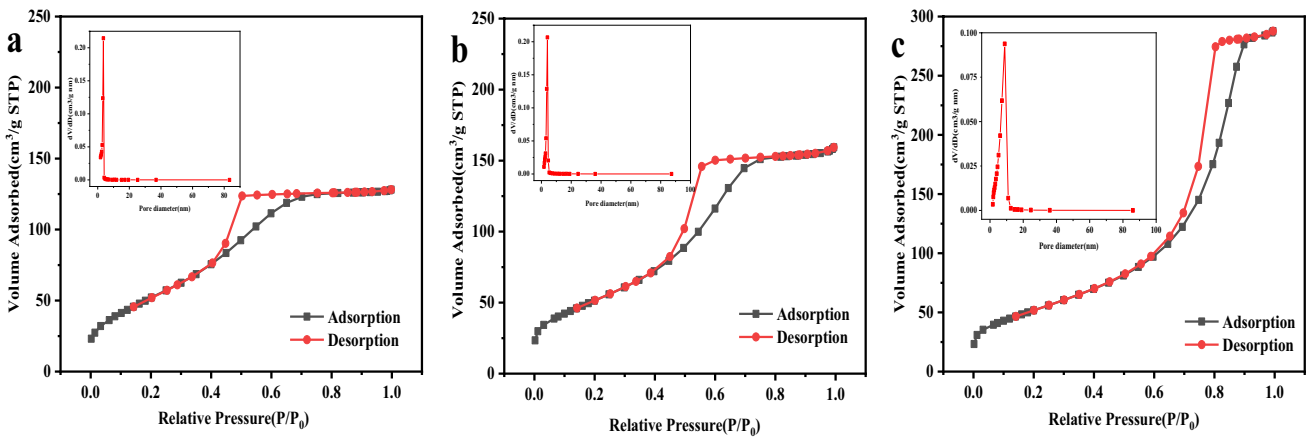

Fig. 2 N_2 adsorption-desorption isotherms and pore size distributions of **a** FO, **b** FCBO, and **c** FCCTO

suggest complex pore structures. The FCCTO exhibits an H_1-type hysteresia loop, indicating the presence of cylindrical pores with uniform pore size distribution and open ends. This confirms that FCCTO is a mesoporous material with relatively narrow pore size distribution, primarily formed by the aggregation of uniformly sized spherical particles, providing abundant binding sites for As(III) adsorption.

Adsorbents' phase and crystallinity were assessed using XRD (Fig. 3). All nanocomposites exhibit low crystallinity. Fe_2O_3 can be well linked to the broad characteristic peaks at 2θ= 32.98° (Wei et al. 2017). The (111), (222), and (311) cubic planes of CeO_2 can be used to describe the peaks at 2θ = 28.66°, 47.69°, and 56.59° (Lashanizadegan et al. 2019). CuO mainly exists in amorphous form since no evident characteristic peak found. The amorphous structure of FO, FCBO, and FCCTO gives rise to a large amount of surface area and adsorption sites. Compared to FCCTO, there was no obvious change in the crystalline phase of FCCTO after As(III) adsorption.

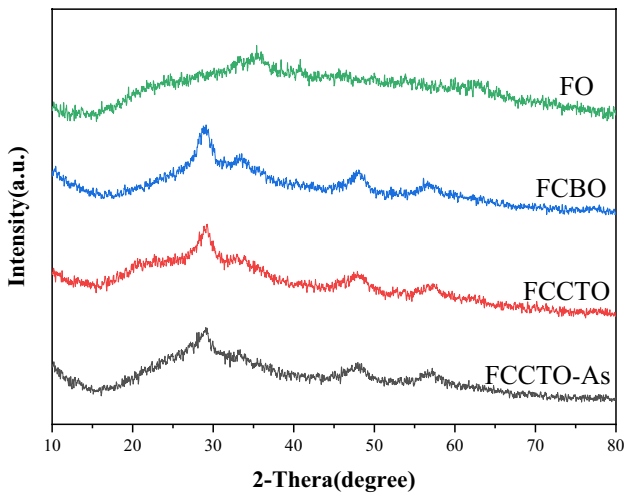

Fig. 3 XRD patterns for the FO, FCBO, FCCTO, and FCCTO after As(III) adsorption

Effect of adsorbent dosage and initial solution pH

As(III) adsorption equilibrium was significantly impacted by the adsorbent's dosage (Fig. 4). When the dose of FCCTO increased from 0.1 to 1.5g/L, the removal efficiency rose from 46.8 to 99.9%, while the adsorption capacity declined from 93.58 to 13.32 mg/g. The increase of removal rate was due to the increase of adsorption sites with the increase of dosage. At the same time, as the effective adsorption sites were decreasing, the excess of adsorption sites drove the decreasing adsorption capacity. The adsorbent dose in the subsequent experiment was adjusted at 0.4 g/L to simultaneously satisfy the needs of economic benefit and adsorption

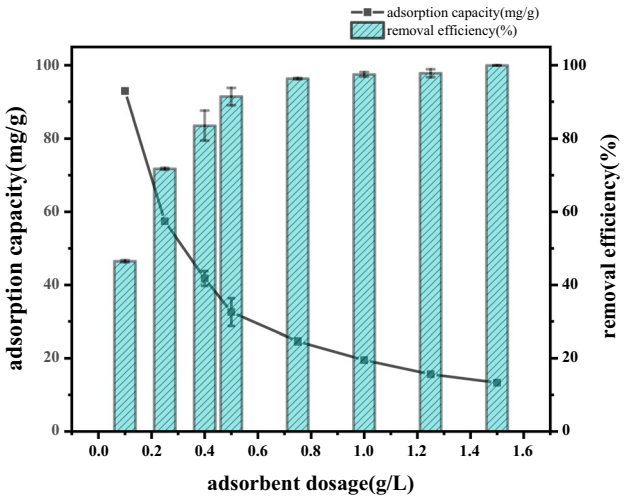

Fig. 4 The effect of FCCTO dosage on As(III) removal. (pH=7.0, C_0=20 mg/L, T=298 K)

effect. As(III) was being removed from the system at a rate of 89.26%, while the adsorption capacity was 44.63 mg/g.

The As(III) adsorption capacity of FO, FCBO, and FCCTO were affected by an initial solution pH in the range of 3 to 11 (Fig. 5a). All adsorption showed similar pH dependence, attributed to the change of arsenic speciation in solution and adsorbents' zeta potential (Fig. 5b) (Chen et al. 2013). The pH_{PZC} of FO, FCBO, and FCCTO can be obtained as 6.98, 6.70, and 6.57, respectively. While the pH raised from 8 to 11, the adsorption performance drops sharply, and there was a sharp increase from 3 to 4. All adsorbents showed good removal capability over a broad pH range of 4 to 8. Metal oxides often achieve their maximum capacity at pH similar to pK_{a1} of the acid, and the pK_{a1} of arsenious acid is 9.2. However, the XPS results demonstrated the presence of As(III) oxidation during the adsorption by FCBO and FCCTO (Fig. 14a), so the $HAsO_4^{2-}$ in the solution gradually increases when pH > 7 (Fig. 6b). Due to the electrostatic repulsion between the arsenic ion and the surface charge of the material, the adsorption capacity decreases continuously. At lower pH values, the As(III) exists as neutral molecules, such as H3AsO3. The adsorption capabilities of FCBO and FCCTO significantly decreased at pH 3 due to the partial dissolution of Ce metal oxides in acidic environment, which resulted in a reduction of surface active sites.

Adsorption kinetics

The sorption kinetics of FCCTO were explored by analyzing the As(III) concentration of solution samples at different contact time (Fig. 7). The rate of As(III) sorption was quick for the first 30 min before slowing. FCCTO and FCBO have

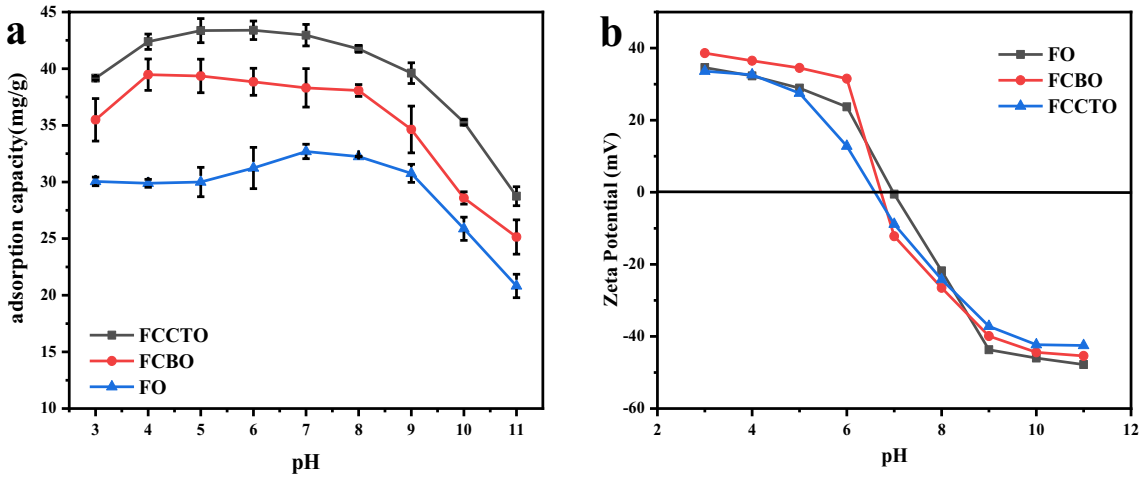

Fig. 5 **a** The effect of pH for As(III) removal on FO, FCBO, and FCCTO (dosage=0.4 g/L, C_0=20 mg/L, T=298 K); **b** the zeta potential of FO, FCBO, and FCCTO at different pH

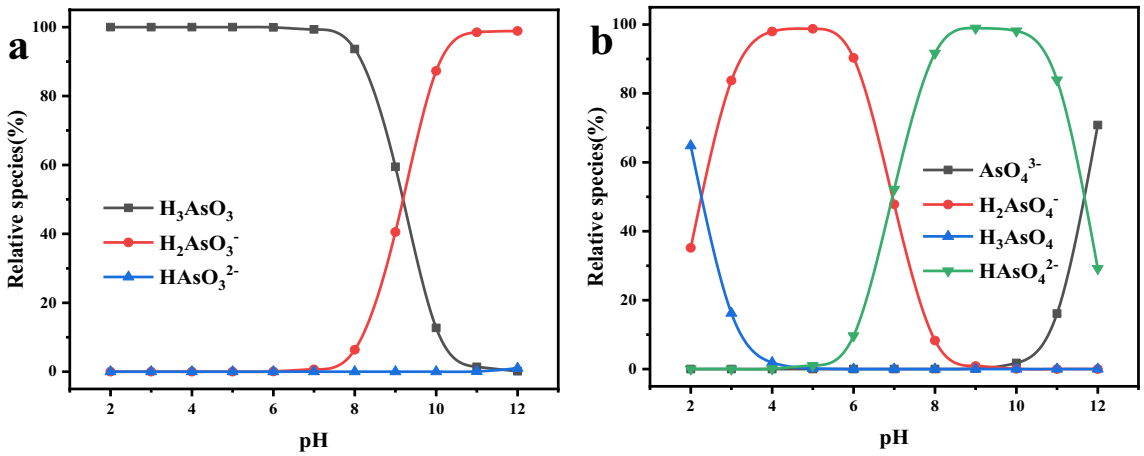

Fig. 6 Distribution of **a** As(III) and b As(V) species as variable pH calculated by Visual MINTEQ(ver.3.1.)

similar trend, while FO's rapid rising period only lasts for a short time (20 min). FCCTO have better adsorption performance than binary oxide and unitary oxide due to synergistic effect (Zheng et al. 2020), which was also reported that the adsorption performance is optimal when the Cu:Fe ratio is 1:3 for As(III) and 1:2 for As(V) (Zhang et al. 2013).

The pseudo-first-order and pseudo-second-order models were utilized to describe the As(III) adsorption behavior (Liu et al. 2021; Zhao et al. 2014). The calculated Q_e of the pseudo-second-order model was much closely matched to the experimental value Q_e (Table 2), and its correlation coefficient were 0.981, 0.996, and 0.992 for FO, FCBO, and FCCTO, respectively. Thus, the chemical adsorption is dominant in the procedure of As(III) adsorption on FCCTO.

The plots fitted by the intra-particle diffusion model showed piecewise linearity, and three stages will take place in the process: (1) rapid initial sorption of As(III) from the solution to sorbent surfaces, (2) sluggish diffusion into the adsorbent's porous structure, and (3) As(III) adsorption on the surfaces of sorbents. The particle diffusion slowed down with the decreasing of As(III) concentration, which was consistent with the widely accepted adsorption process. As shown by the sequence of diffused rate constants (Table 3), $k_{p1}>k_{p2}>k_{p3}$, indicated intra-particle diffusion and film diffusion certificated the whole procedures. The highest rate constant of FCCTO revealed Fe-Ce-Cu ternary–doped metal oxide has different structural characteristics for boosting As(III) adsorption.

Adsorption isotherms

Sorption isotherm experiments were conducted at 298, 308, and 318 K to evaluate the impact of the As(III) starting concentration on the removal capability (Fig. 8). The absorbed

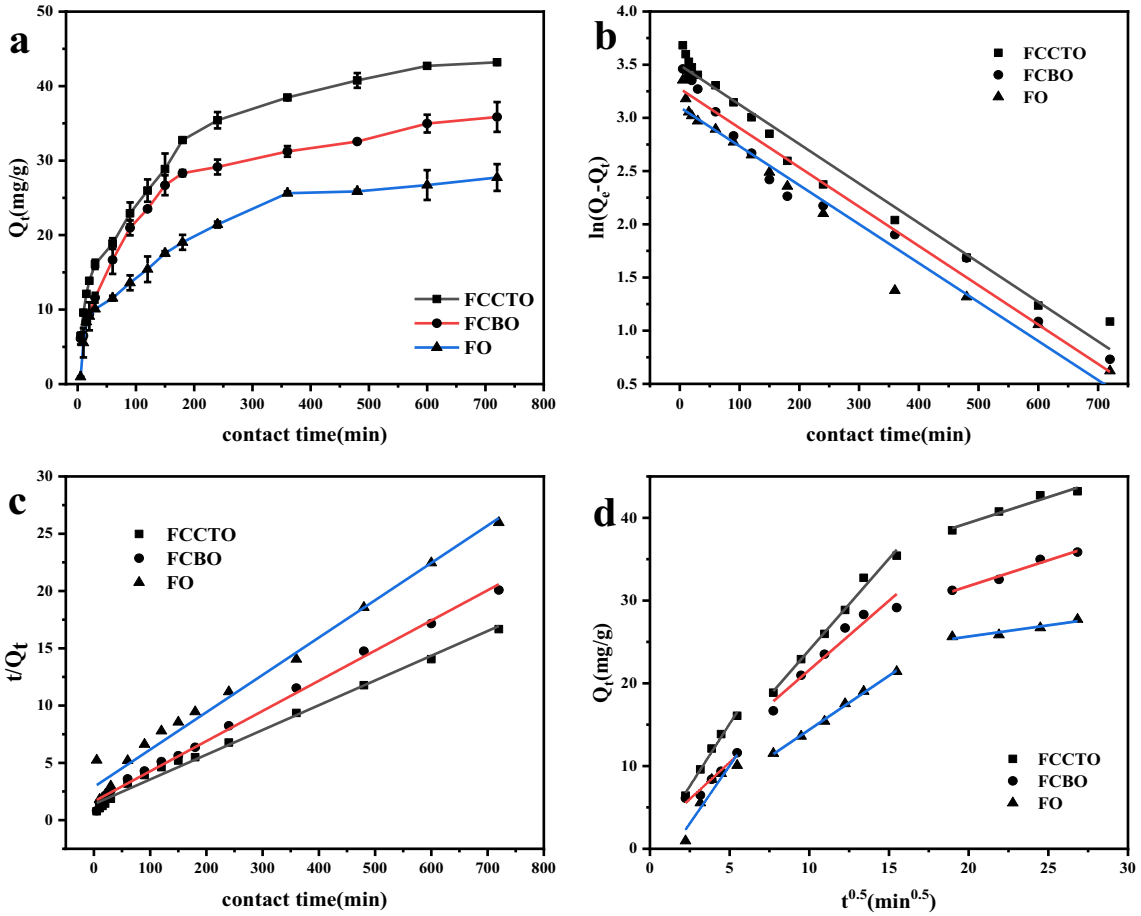

Fig. 7 **a** The adsorption kinetic of As(III) on FO, FCBO, and FCCTO (dosage=0.4 g/L, pH=7, C_0=20 mg/L, T=298 K). **b** Linear fit of pseudo-first-order model of kinetic data. **c** Linear fit of pseudo-second-order model of kinetic data. **d** Kinetic data plotted using the intra-particle diffusion model

Table 2 Kinetic parameters of dynamic fit of As(III) on FO, FCBO, and FCCTO

Adsorbent	$Q_{e,exp}$	Pseudo-first-order			Pseudo-second-order		
	(mg/g)	k_1(1/min)	$Q_{e,cal}$ (mg/g)	R^2	k_2 (g/mg·min)	$Q_{e,cal}$ (mg/g)	R^2
FO	29.591	$3.661*10^{-3}$	22.205	0.966	$3.664*10^{-4}$	30.684	0.981
FCBO	37.933	$3.723*10^{-3}$	26.438	0.950	$4.243*10^{-4}$	37.979	0.996
FCCTO	46.161	$3.712*10^{-3}$	32.992	0.972	$3.343*10^{-4}$	46.318	0.992

Table 3 Intra-particle diffusion model coefficients of As(III) on FO, FCBO, and FCCTO

Adsorbent	Film diffusion			Intra-particle diffusion			Equilibrium stage		
	k_{p1}	C_1	R^2	k_{p2}	C_2	R^2	k_{p3}	C_3	R^2
FO	2.797	−3.941	0.8424	1.305	1.337	0.9968	0.270	20.260	0.8712
FCBO	1.771	1.584	0.9373	1.675	4.860	0.9244	0.623	19.292	0.9602
FCCTO	3.016	0.018	0.9850	2.208	1.944	0.9868	0.623	26.929	0.9365

As(III) on adsorbent were increased as gradient starting concentration rose from 10 to 200 mg/L.

The sorption results were fitted with the Langmuir, Freundlich, Tempkin, and D-R kinetic models (Fig. 9) (Hu and Zhang 2019), and the equilibrium data were obtained (Table 4).

The high correlation coefficients ($R^2 > 0.991$) indicated that Langmuir isotherm model is more suited than other three

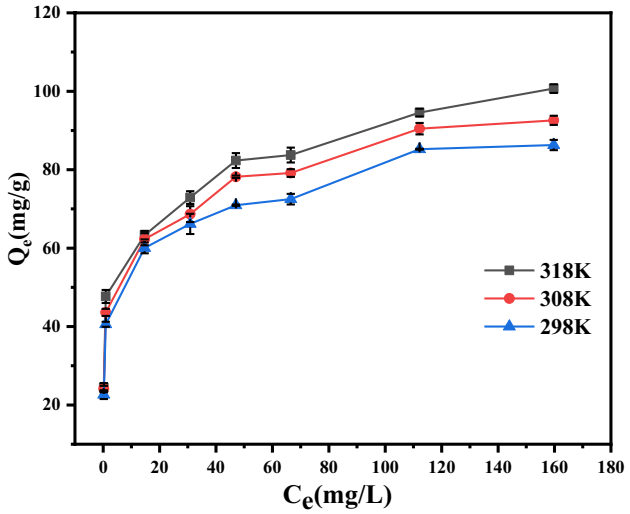

Fig. 8 Adsorption isotherm of As(III) on FCCTO at different temperatures (dosage=0.4 g/L, pH=7.0)

models. The maximal adsorption capabilities at 298, 308, and 318 K predicted to be 88.89, 94.70, and 101.5 mg/g, respectively, which is superior to many sorbents (Table 5). The As(III) adsorption on FCCTO belonged to monolayer adsorption on the homogeneous surface. The fact that the adsorption capacity increases as the temperature does, indicating that the adsorption on FCCTO is an endothermic reaction.

The preferred degree of removal process is often estimated using the dimensionless separation constant R_L. When the R_L is between 0 and 1, it certificates that the adsorption is beneficial. When the starting concentration varied from 10 to 200 mg/L at 298, 308, and 318 K, the calculated R_L values of FCCTO are 0.0394–0.2910, 0.0343–0.2621, and 0.0340–0.2604, it shows that FCCTO is beneficial to As(III).

The adsorption thermodynamics of FCCTO adsorbing As(III) by changing the adsorption temperature is depicted in Fig. 10. Then, As(III) was adsorbing in greater quantities as the adsorption temperature was raised. To ascertain if the As(III) adsorption process on FCCTO is spontaneous and

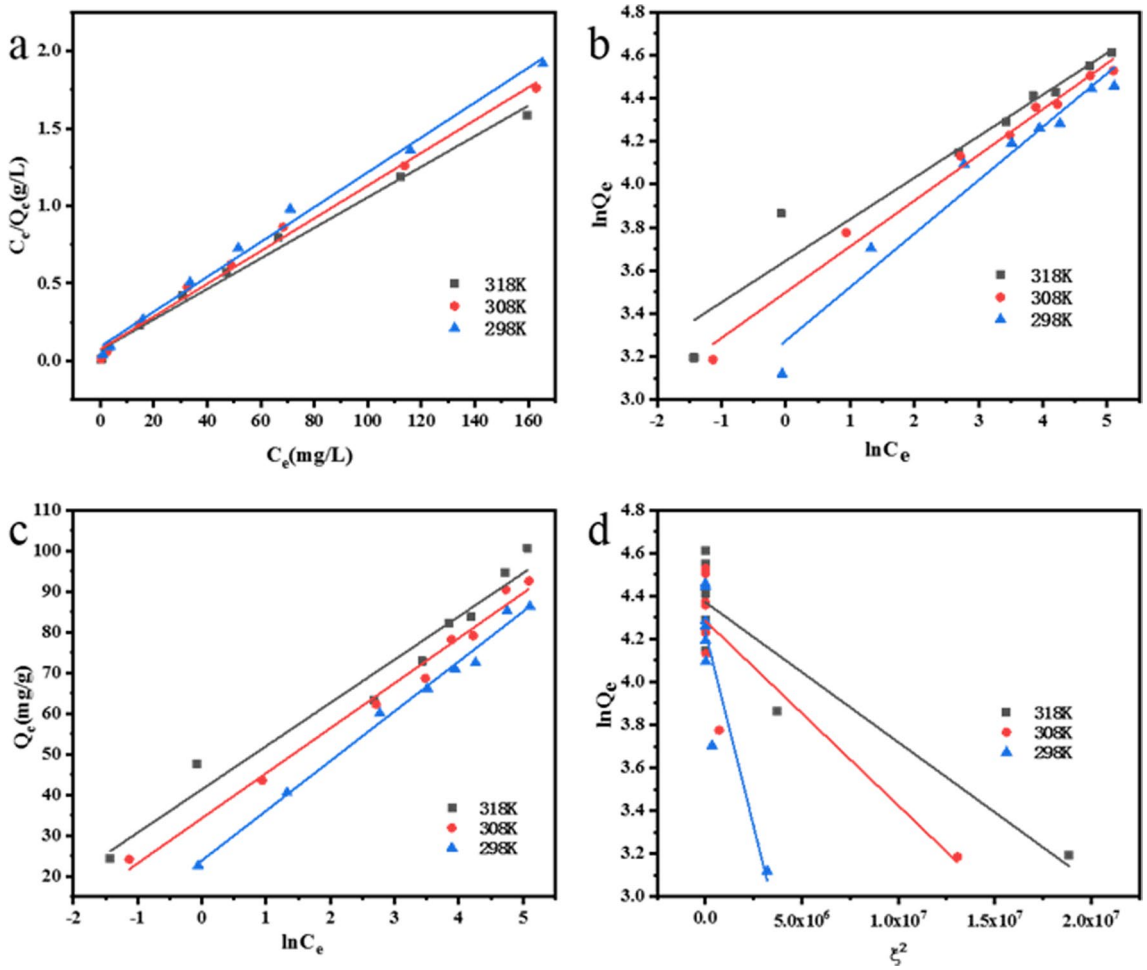

Fig. 9 **a** The linear graphs of **a** Langmuir, **b** Freundlich, **c** Tempkin, and **d** D-R adsorption isotherm models (dosage=0.4 g/L, pH= 7.0, contact time=12 h)

Table 4 Isotherm parameters of As(III) on FCCTO at different temperatures

Isotherm model	Parameters	298 K	308 K	318 K
Langmuir	Q_m (mg/g)	88.89	94.70	101.52
	b (L/mg)	0.1218	0.1407	0.1420
	R^2	0.9933	0.9937	0.9910
Freundlich	K_f (mg/g (L/mg) 1/n)	26.42	33.09	38.29
	n	4.024	4.701	5.180
	R^2	0.9584	0.9868	0.9426
Tempkin	AT (L/mg)	7.06	22.22	49.17
	BT (J/mol)	12.23	11.06	10.62
	R^2	0.9909	0.9869	0.9634
D-R	Q_s (mg/g)	68.80	72.544	79.161
	K_e (mol^2/kJ^2)	3.608E-7	8.596E-8	6.522E-8
	E (kJ/mol)	1177	2412	2769
	R^2	0.8005	0.7578	0.8540

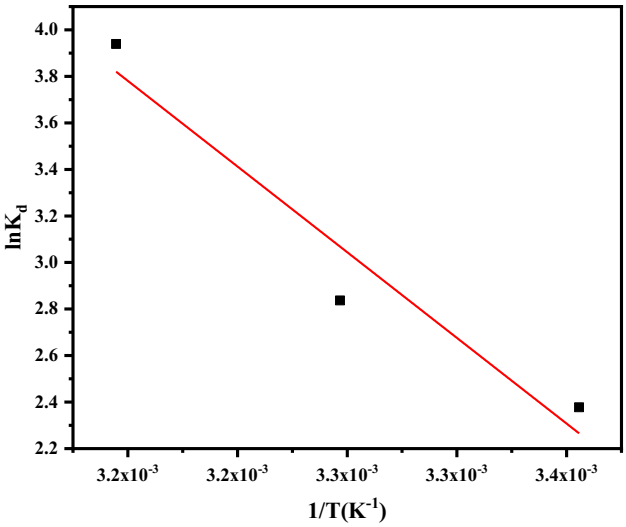

Fig. 10 Thermodynamics graph for As(III) removal on FCCTO (dosage=0.4 g/L, C_0=20mg/L, pH=7)

endothermic, the thermodynamic parameters standard free energy change (ΔG^0), standard enthalpy change (ΔH^0), and standard entropy change (ΔS^0) were examined. The value of ΔS^0 and ΔH^0 was calculate through fitting each linear regression in Table 6.

The positive ΔH^0 value verified that the As(III) removal on FCCTO was endothermic in essence. ΔG^0 recorded negative value indicated that the interaction of As(III) adsorbed by FCCTO is spontaneous; furthermore, As(III) is more amenable to adsorption at higher adsorption temperatures. The positive ΔS^0 values reflected the increased randomness in the adsorption process. The abovementioned confirmed there is a spontaneous and endothermic process in the adsorption of As(III) on FCCTO.

Table 6 Thermodynamics parameters for adsorption of As(III) on FCCTO

T (K)	ΔG^0 (kJ/mol)	ΔH^0 (kJ/mol)	ΔS^0 (J/mol)
298	−5.613	61.244	224.352
308	−7.856		
318	−10.100		

Effect of coexisting anions on arsenite adsorption

The effects of anions such as SO_4^{2-}, Cl^-, CO_3^{2-}, PO_4^{3-}, and SiO_3^{2-} coexistence on the As(III) sorption of FCCTO were investigated (Fig. 11). The presence of SO_4^{2-} and Cl^- has no significantly negatively impacted on As(III) removal while CO_3^{2-} only marginally inhibits while concentration was above 10 mmol/L. The presence of PO_4^{3-} and SiO_3^{2-} strongly inhibits As(III) sorption due to the fact that phosphatic, silicon, and arsenic ions have similar molecular structures, and PO_4^{3-} could form stable inner sphere complexes with the surface hydroxyl group of iron oxides (Sigdel et al. 2016).

Table 5 Comparison of the maximum adsorption capacity of As(III) on FCCTO with various adsorbents published in literatures

Adsorbents	Conditions	Q_m(mg/g)	Ref.
Ceria nanoparticles	T=323K, pH=7.0, D=5.0g/L	18.15	Feng et al. (2012)
CuO nanoparticles	T=298K, pH=8.0, D=2.0g/L	26.9	Martinson and Reddy (2009)
Ce-Fe metal oxides with CNT	T=298K, pH=7.5, D=0.2g/L	28.7	Chen et al. (2013)
Cu-doped Fe_3O_4	T=298K, pH=5.0, D=0.5g/L	37.97	Wang et al. (2015)
Iron(III)–cerium(IV) oxide	T=303K, pH=7.0, D=0.4g/L	86.29	Basu et al. (2013)
Cerium-manganese binary oxide	T=298K, pH=7.0, D=0.2g/L	97.7	Chen et al. (2018)
Fe-Mn binary oxide	T=298K, pH=5.0, D=0.2g/L	100.4	Zhang et al. (2007)
Fe-Ti-Mn composite oxide	T=298K, pH=7.0, D=0.2g/L	119.6	Zhang et al. (2018)
Fe-Mn-Cu ternary oxide	T=298K, pH=7.0, D=0.3g/L	204.79	Wu et al. (2021)
FCCTO	T=323K, pH=7.0, D=0.4g/L	101.5	This study

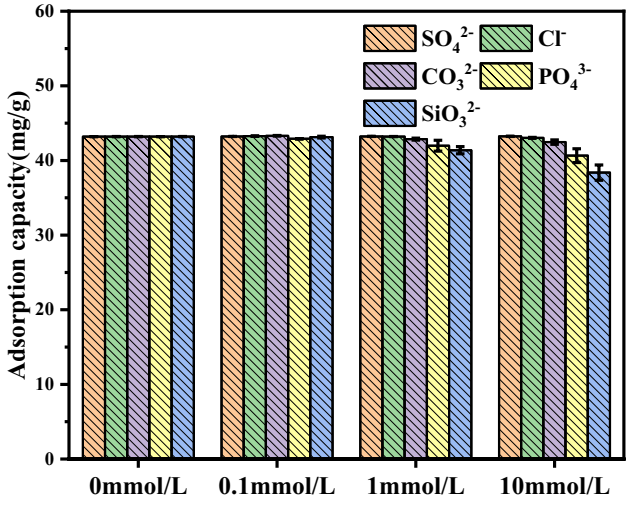

Fig. 11 The impacts of coexisting anions on the As(III) removal by using FCCTO (dosage=0.4 g/L, C_0=20mg/L, pH=7, contact time=12 h)

Reusability and stability

The reusability was evaluated through five consecutive recycling cycles (Fig. 12a). With an increase in cycles, the adsorption and desorption capacities gradually reduced. And the close values of adsorption and desorption capacities may mean that the pore blockage during regeneration is not obvious, which is conducive to the formation of good regeneration performance. The adsorption rate remained above 60% after five cycles and NaOH solution was a simple way to renew FCCTO. According to the XPS data (Fig. 14), the content of hydroxyl group and tetravalent cerium decreased after five cycles result in the decrease of arsenic binding sites and cerium oxidation ability. The generation of a large amount of lattice oxygen proved that there is a transfer of oxygen electrons in the adsorption process.

To investigate the stability of FO, FCBO, and FCCTO, the dissolved concentration of metal ions during adsorption process is measured (Fig. 12b). The dissolution concentration of Fe and Ce ions was below 0.11mg/L and 0.04mg/L, and the dissolved amount of heavy metal copper was in trace level. Thus, the prepared materials all have good stability and will cause very little pollution.

Adsorption mechanism

The FTIR (Fig. 13) and XPS (Fig. 14) spectra of FCCTO before and after adsorption were obtained to explore the mechanisms. The broad band between 3000 and 3600 cm^{-1} were related to the stretching vibrations peak of the O–H groups including lattice and adsorbed water (Wen et al. 2018). After As(III) adsorption, the signal from the −OH group is slightly weaker, indicating that there is complexation between the As(III) and −OH groups. And the Ce–OH bending vibrations at 1059 and 1533cm^{-1} became weaker than before As(III) adsorption (Guo et al. 2011). The adsorbed CO_2 in the atmosphere may be responsible for the 1364 cm^{-1} peak of CO_3^{2-} vibration (Li et al. 2014). Carbonate and hydroxyl groups on FCCTO can displace by arsenate attributed to ion exchange. As(V) adsorption band and the stretching vibration As-O in the range of 650–800 cm^{-1} prove that As is adsorbed and redox reaction occurs during the adsorption procedure (Lin et al. 2017; Mohan et al. 2007). The emergence of As-O-Ce vibration at 829 cm^{-1} shows the inner sphere mechanism of As(III) adsorption.

XPS was applied to certify the oxidation–redox process, the binding energy of As-3d, O-1s, Ce-3d, and Cu-2p

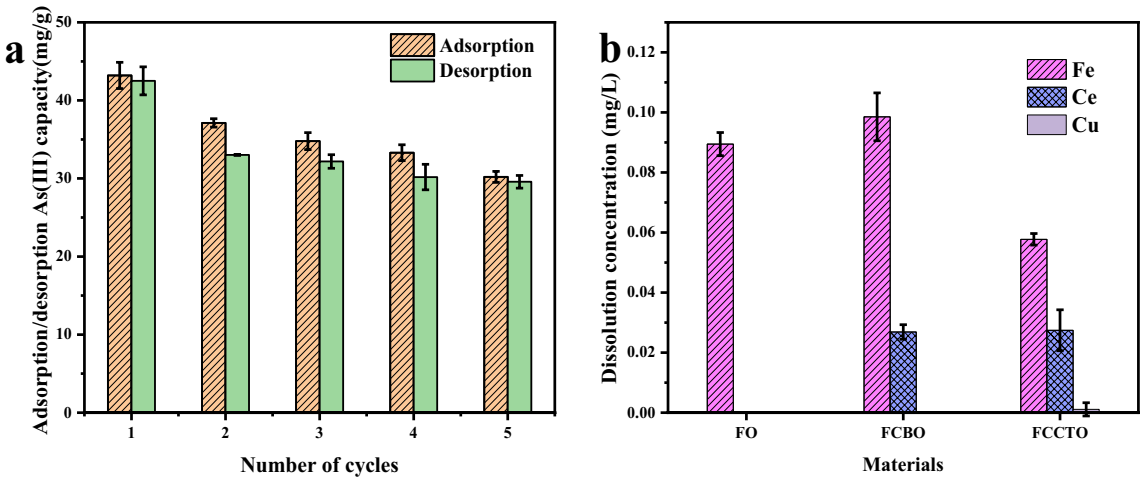

Fig. 12 **a** As(III) adsorption and desorption in five successive regeneration cycles on Fe-Ce-Cu ternary oxide. **b** The dissolution concentration of Fe, Ce, and Cu after As(III) adsorbed by FO, FCBO, and FCCTO (dosage=0.4 g/L, C_0=20mg/L, pH=7)

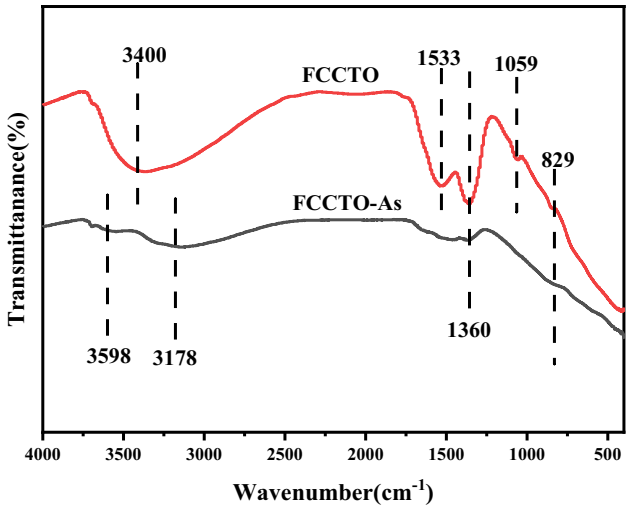

Fig. 13 FTIR spectra of Fe-Ce-Cu ternary oxide before and after As(III) adsorption (dosage=0.4 g/L, C_0=20mg/L, pH=7)

core-level photoelectron spectra. The binding energy (B.E.) at 44.3 and 45.2 eV are associated with As(III) and As(V), respectively. FCCTO showed the excellent oxidation performance than the binary oxide FCBO, and 81.3% trivalent arsenic was definitely oxidized to pentavalent arsenic. The oxidation performance of low-dose copper doping oxides is also quite big different from that of binary oxides as reported.

The O-1s spectra in Fig.14b could be divided into three peaks of adsorbed water (H_2O), hydroxyl (−OH), and lattice oxygen (O^{2-}). By comparing the spectra of oxygen elements before and after As(III) sorption, it can be observed that hydroxyl groups take up an prominent position in the adsorption process, which is similar to the FTIR results. It was certified that O^{2-} are origin from oxygen molecules, which are adsorbed on the FCCTO surface and function as electron transport, and have the ability to oxidize and adsorbed arsenic and dissolve arsenic capably.

By fitting Ce-3d spectra in Fig. 14c, the valence state was examined. Fe-Ce-Cu ternary oxide contains primarily CeO_2 as Ce oxide. The reduction degree of Ce(IV) is not obvious after first adsorption and its content decreased after repeated adsorption. Cu plays a greater role in the oxidation-reduction process. Cu(I) increases from 30.2 to 38.6% while Cu(II) decreases from 69.8 to 61.4% after interaction with As(III). The oxidized As(V) from As(III) was explained to the decrease of Ce(IV) and Cu(II) atoms, related to the catalytic oxidation performance of Ce-Cu oxides (Jin et al. 2020).

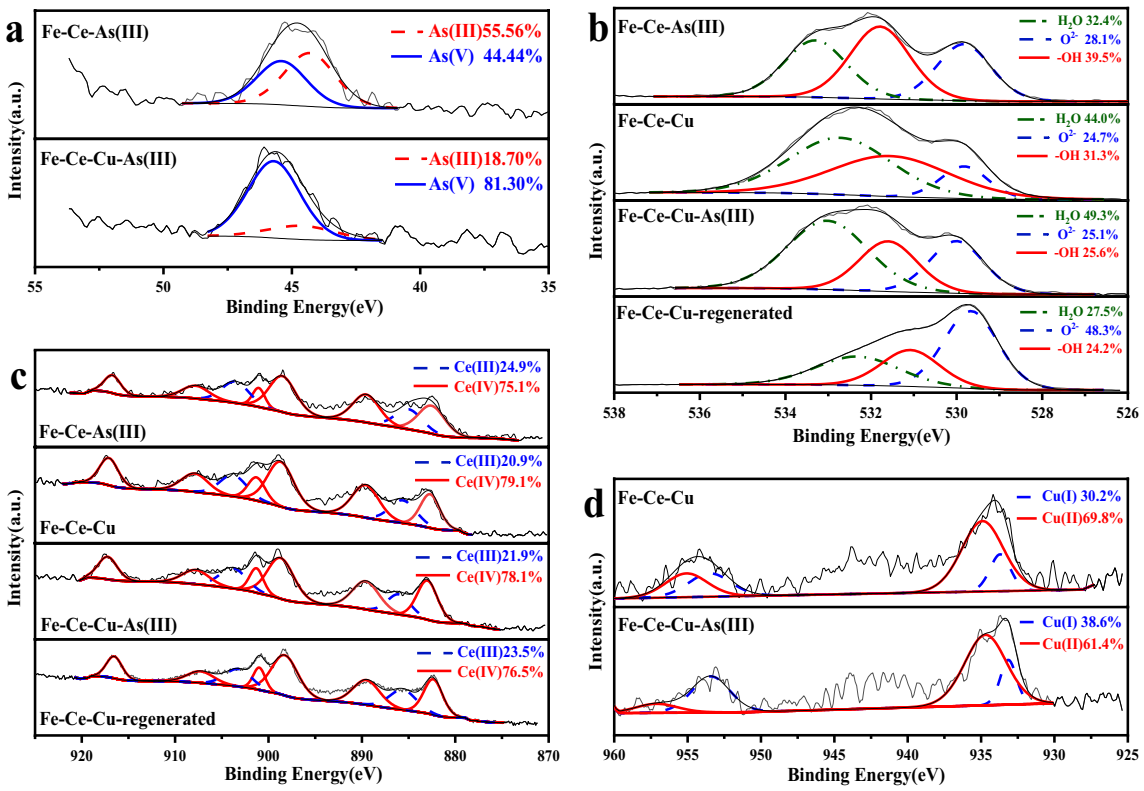

Fig. 14 The XPS spectra of Fe-Ce binary oxide and Fe-Ce-Cu ternary oxide before and after reactions with As(III): **a** As-3d, **b** O-1s, **c** Ce-3d, and **d** Cu-2p (dosage=0.4 g/L, pH= 7.0, contact time=12 h)

Thus, the following As(III) adsorption mechanisms by Fe-Ce-Cu ternary oxide can be inferred from the discussion above: (i)As(III) species would first be transported from solution phase to the interface between solid and water, and formed complexes. (ii) Cu(II) and Ce(IV) are used as oxidants in the adsorption process to conveniently oxidize As(III) to As(V).

Conclusions

Fe-Ce-Cu ternary oxide with a Fe/Ce/Cu molar proportion of 3:0.8:0.5 was effectively prepared by a coprecipitation–calcination technique. The manifested synergistic effect and catalytic oxidation performance of three oxides greatly improves the treatment capacity of As(III) in aqueous. The maximum As(III) adsorption capacity of FCCTO is 101.5mg/g. The adsorbent dosing amount, solution initial pH, contact time, starting As(III) concentration, ambient temperature, and ionic strength were found as critical influence factor for As(III) sorption. The adsorption process of FCCTO was pseudo-second-order kinetic, and the Langmuir model was matched by the adsorption isotherm. Adsorption of As(III) was mediated through surface complexation, redox, and adsorption. After sorption, As(III) was transformed into As(V) in an amount of 81.3%. It was simple to renew the spent Fe-Ce-Cu ternary oxide employing NaOH solution. The Fe-Ce-Cu ternary oxide would be a useful and alternate adsorbent for As(III) adsorption from aquatic ecosystems owing to its convenient synthesis technique, strong arsenic removal efficiency, and simple regeneration.

Author contributions Ying Liu: conceptualization, methodology, data analysis, writing—review and editing, visualization, and validation. Leyi Li: methodology, data collection, review and editing. Xuemei Huang: review and editing. Yaochi Liu: supervision, review and editing, visualization, and validation.

Funding We acknowledge the key Research and Development Projects of Hunan Province (No. 2019WK2031) for financial support of this research.

Data availability The data analyzed in this study are available from the corresponding author on reasonable request.

Declarations

Ethics approval and consent to participate Not applicable.

Consent for publication Not applicable.

Competing interests The authors declare no competing interests.

References

Ayub A, Raza ZA, Majeed MI, Tariq MR, Irfan A (2020) Development of sustainable magnetic chitosan biosorbent beads for kinetic remediation of arsenic contaminated water. Int J Biol Macromol 163:603–617. https://doi.org/10.1016/j.ijbiomac.2020.06.287

Ayub A, Srithilat K, Fatima I, Panduro-Tenazoa NM, Ahmed I, Akhtar MU, Ahmad K, Muhammad A (2022) Arsenic in drinking water: overview of removal strategies and role of chitosan biosorbent for its remediation. Environ Sci Pollut R 29(43):64312–64344. https://doi.org/10.1007/s11356-022-21988-z

Basu T, Nandi D, Sen P, Ghosh UC (2013) Equilibrium modeling of As(III,V) sorption in the absence/presence of some groundwater occurring ions by iron(III)–cerium(IV) oxide nanoparticle agglomerates: a mechanistic approach of surface interaction. Chem Eng J 228:665–678. https://doi.org/10.1016/j.cej.2013.05.037

Çermikli E, Şen F, Altıok E, Wolska J, Cyganowski P, Kabay N, Bryjak M, Arda M, Yüksel M (2020) Performances of novel chelating ion exchange resins for boron and arsenic removal from saline geothermal water using adsorption-membrane filtration hybrid process. Desalination 491:114504. https://doi.org/10.1016/j.desal.2020.114504

Chen B, Zhu ZL, Ma J, Qiu YL, Chen JH (2013) Surfactant assisted Ce–Fe mixed oxide decorated multiwalled carbon nanotubes and their arsenic adsorption performance. J Mater Chem A 1(37):11355–11367. https://doi.org/10.1039/c3ta11827d

Chen J, Wang JY, Zhang GS, Wu QY, Wang DT (2018) Facile fabrication of nanostructured cerium-manganese binary oxide for enhanced arsenite removal from water. Chem Eng J 334:1518–1526. https://doi.org/10.1016/j.cej.2017.11.062

Chen L, Zhang KS, He JY, Cai XG, Xu WH, Liu JH (2016) Performance and mechanism of hierarchically porous Ce-Zr oxide nanospheres encapsulated calcium alginate beads for fluoride removal from water. RSC Adv 6(43):36296–36306. https://doi.org/10.1039/c6ra01337f

Dodd MC, Vu ND, Ammann A, Le VC, Kissner R, Pham HV, Cao TH, Berg M, Gunten AV (2006) Kinetics and mechanistic aspects of As(III) oxidation by aqueous chlorine, chloramines, and ozone: relevance to drinking water treatment. Environ Sci Technol 40(10):3285–3292. https://doi.org/10.1021/es0524999

Feng QZ, Zhang ZY, Ma YH, He X, Zhao YL, Chai ZF (2012) Adsorption and desorption characteristics of arsenic onto ceria nanoparticles. Nanoscale Res Lett 7:1–8. https://doi.org/10.1186/1556-276X-7-84

Guo HC, Li WJ, Wang HY, Zhang JH, Liu Y, Zhou Y (2011) A study of phosphate adsorption by different temperature treated hydrous cerium oxides. Rare Metals 30(1):58–62. https://doi.org/10.1007/s12598-011-0197-5

Gupta AD, Rene ER, Giri BS, Pandey A, Singh H (2021) Adsorptive and photocatalytic properties of metal oxides towards arsenic remediation from water: a review. J Environ Chem Eng 9(6):106376. https://doi.org/10.1016/j.jece.2021.106376

Han YS, Kim SH, Jang JY, Ji S (2022) Arsenic removal characteristics of natural Mn-Fe binary coating on waste filter sand from a water treatment facility. Environ Sci Pollut R 29(2):2136–2145. https://doi.org/10.1007/s11356-021-15580-0

Hoang VA, Yoshizuka K, Nishihama S (2022) Oxidative adsorption of arsenic from water environment by activated carbon modified with cerium oxide/hydroxide. Chem Eng Res Des 186:161–173. https://doi.org/10.1016/j.cherd.2022.08.006

Hu QL, Zhang ZY (2019) Application of Dubinin-Radushkevich isotherm model at the solid/solution interface: a theoretical analysis. J Mol Liq 277:646–648. https://doi.org/10.1016/j.molliq.2019.01.005

Huang YL, Tian XK, Nie YL, Yang C, Wang YX (2018) Enhanced peroxymonosulfate activation for phenol degradation over MnO_2 at pH 3.5-9.0 via Cu(II) substitution. J Hazard Mater 360:303–310. https://doi.org/10.1016/j.jhazmat.2018.08.028

Jin LF, Chai LY, Song TT, Yang WC, Wang HY (2020) Preparation of magnetic Fe_3O_4@Cu/Ce microspheres for efficient catalytic oxidation co-adsorption of arsenic(III). J Cent South Univ 27(04):1176–1185. https://doi.org/10.1007/s11771-020-4358-2

Kim MJ, Nriagu J (2000) Oxidation of arsenite in groundwater using ozone and oxygen. Sci Total Environ 247(1):71–79. https://doi.org/10.1016/S0048-9697(99)00470-2

Koseoglu P, Yoshizuka K, Nishihama S, Yuksel U, Kabay N (2011) Removal of boron and arsenic from geothermal water in Kyushu Island, Japan, by using selective ion exchange resins. Solvent Extr Ion Exc 29(3):440–457. https://doi.org/10.1080/07366299.2011.573448

Lashanizadegan M, Esfandiari Z, Mirzazadeh H (2019) Evaluation performance of Fe–Mn–Ce–O mixed metal oxides and Fe–Mn–Ce–O/Montmorillonite for adsorption of azo dyes in aqueous solution and oxidation reaction. Mater Res Express 6(12):125028. https://doi.org/10.1088/2053-1591/ab5550

Li GL, Gao S, Zhang GS, Zhang XW (2014) Enhanced adsorption of phosphate from aqueous solution by nanostructured iron(III)-copper(II) binary oxides. Chem Eng J 235:124–131. https://doi.org/10.1016/j.cej.2013.09.021

Li RH, Yang WY, Gao S, Shang JK, Li Q (2021) Hydrous cerium oxides coated glass fiber for efficient and long-lasting arsenic removal from drinking water. J Adv Ceramics 10(2):247–257. https://doi.org/10.1007/s40145-020-0435-0

Li X, He K, Pan BC, Zhang SJ, Lu L, Zhang WM (2012) Efficient As(III) removal by macroporous anion exchanger-supported Fe–Mn binary oxide: bbehavior and mechanism. Chem Eng J 193-194(15):131–138. https://doi.org/10.1016/j.cej.2012.04.036

Lin L, Qiu WW, Wang D, Huang Q, Song ZG, Chaud HW (2017) Arsenic removal in aqueous solution by a novel Fe-Mn modified biochar composite: characterization and mechanism. Ecotox Environ Safe 144:514–521. https://doi.org/10.1016/j.ecoenv.2017.06.063

Lin PF, Zhang XJ, Yang HW, Li Y, Chen C (2015) Applying chemical sedimentation process in drinking water treatment plant to address the emergent arsenic spills in water sources. Front Env Sci Eng 9(1):50–57. https://doi.org/10.1007/s11783-014-0733-2

Liu J, Ren SX, Cao JL, Tsang DCW, Beiyuan JZ, Peng YT, Fang F, She JY, Yin ML, Shen NP, Wang J (2021) Highly efficient removal of thallium in wastewater by $MnFe_2O_4$-biochar composite. J Hazard Mater 401:123311. https://doi.org/10.1016/j.jhazmat.2020.123311

Luo XB, Wang CC, Luo SL, Dong RZ, Tu XM, Zeng GS (2012) Adsorption of As (III) and As (V) from water using magnetite Fe_3O_4-reduced graphite oxide–MnO_2 nanocomposites. Chem Eng J 187:45–52. https://doi.org/10.1016/j.cej.2012.01.073

Luo XB, Wang CC, Wang LC, Deng F, Luo SL, Tu XM, Au C (2013) Nanocomposites of graphene oxide-hydrated zirconium oxide for simultaneous removal of As(III) and As(V) from water. Chem Eng J 220:98–106. https://doi.org/10.1016/j.cej.2013.01.017

Martinson CA, Reddy KJ (2009) Adsorption of arsenic(III) and arsenic(V) by cupric oxide nanoparticles. J Colloid Interf Sci 336(2):406–411. https://doi.org/10.1016/j.jcis.2009.04.075

Masuda H (2018) Arsenic cycling in the Earth's crust and hydrosphere: interaction between naturally occurring arsenic and human activities. Prog Earth Planet Sc 5(1):68. https://doi.org/10.1186/s40645-018-0224-3

Mohan D, Pittman CU, Bricka M, Smith F, Yancey B, Mohammad J, Steele PH, Alexandre-Franco MF, Gómez-Serrano V, Gong H (2007) Sorption of arsenic, cadmium, and lead by chars produced from fast pyrolysis of wood and bark during bio-oil production. J Colloid Interf Sci 310:57–73. https://doi.org/10.1016/j.jcis.2007.01.020

Moretti E, Storaro L, Talon A, Riello P, Molina AI, Castellón ER (2015) 3-D flower like Ce–Zr–Cu mixed oxide systems in the CO preferential oxidation (CO-PROX): effect of catalyst composition. Appl Catal B-Environ 168−169:385–395. https://doi.org/10.1016/j.apcatb.2014.12.032

Nanseu-Njiki C, Alonzo V, Bartak D, Ngameni E, Darchen A (2007) Electrolytic arsenic removal for recycling of washing solutions in a remediation process of CCA-treated wood. Sci Total Environ 384(1-3):48–54. https://doi.org/10.1016/j.scitotenv.2007.04.043

Peng XJ, Luan ZK, Ding J, Di ZC, Li YH, Tian BH (2005) Ceria nanoparticles supported on carbon nanotubes for the removal of arsenate from water. Mater Lett 59(4):399–403. https://doi.org/10.1016/j.matlet.2004.05.090

Shan SJ, Chen ZH, Koh KY, Wang W, Wu JY, Chen JP, Cui FY (2022) Decontamination of arsenite by a nano-sized lanthanum peroxide composite through a simultaneous treatment process combined with spontaneously catalytic oxidation and adsorption reactions. Chem Eng J 435(3):135082. https://doi.org/10.1016/j.cej.2022.135082

Sherlala AIA, Raman AAA, Bello MM, Buthiyappan A (2019) Adsorption of arsenic using chitosan magnetic graphene oxide nanocomposite. J Environ Manage 246:547–556. https://doi.org/10.1016/j.jenvman.2019.05.117

Siddiqui SI, Chaudhry SA (2017) Iron oxide and its modified forms as an adsorbent for arsenic removal: a comprehensive recent advancement. Process Saf Environ 111:592–626. https://doi.org/10.1016/j.psep.2017.08.009

Sigdel A, Park J, Kwak H, Park PK (2016) Arsenic removal from aqueous solutions by adsorption onto hydrous iron oxide-impregnated alginate beads. J Ind Eng Chem 35:277–286. https://doi.org/10.1016/j.jiec.2016.01.005

Song WY, Yamaki T, Yamaji N, Ko D, Jung KH, Fujii-Kashino M, An G, Martinoia E, Lee Y, Ma JF (2014) A rice ABC transporter, OsABCC1, reduces arsenic accumulation in the grain. P Nati A Sci 111(44):15699–15704. https://doi.org/10.1073/pnas.1414968111

Sorlini S, Gialdini F (2010) Conventional oxidation treatments for the removal of arsenic with chlorine dioxide, hypochlorite, potassium permanganate and monochloramine. Water Res 44(19):5653–5659. https://doi.org/10.1016/j.watres.2010.06.032

Sun WZ, Li Q, Gao SA, Shang JK (2012) Exceptional arsenic adsorption performance of hydrous cerium oxide nanoparticles: Part B. Integration with silica monoliths and dynamic treatment. Chem Eng J 185-186:136–143. https://doi.org/10.1016/j.cej.2012.01.060

Wang T, Yang WC, Song TT, Li CF, Zhang LY, Wang HY, Chai LY (2015) Cu doped Fe_3O_4 magnetic adsorbent for arsenic: synthesis, property, and sorption application. RSC Adv 5(62):50011–50018. https://doi.org/10.1039/c5ra03951g

Wang TN, Jiao YH, He MC, Ouyang W, Lin CY, Liu XT (2022) Facile co-removal of As(V) and Sb(V) from aqueous solution using Fe-Cu binary oxides: structural modification and self-driven force field of copper oxides. Sci Total Environ 803:150084–150084. https://doi.org/10.1016/j.scitotenv.2021.150084

Wei DH, Sun YW, Xu D, Li WZ, Zhao XC, Tao XQ, Zeng SY (2017) Mesoporous Fe_2O_3 nanomaterials from natural rust for lithium storage. J Mater Sci-Mater El 28(24):19098–19104. https://doi.org/10.1007/s10854-017-7864-8

Wen ZP, Ke J, Xu JL, Guo S, Zhang YL, Chen R (2018) One-step facile hydrothermal synthesis of flowerlike Ce/Fe bimetallic oxides for efficient As(V) and Cr(VI) remediation: performance and mechanism. Chem Eng J 343:416–426. https://doi.org/10.1016/j.cej.2018.03.034

Wen ZP, Lu J, Zhang YL, Cheng G, Huang SN, Chen J, Xu R, Ming YA, Wang YR, Chen R (2020) Facile inverse micelle fabrication of magnetic ordered mesoporous iron cerium bimetal oxides with excellent performance for arsenic removal from water. J Hazard

Mater 383:121172.1–121172.12. https://doi.org/10.1016/j.jhazmat.2019.121172

World Health Organization (2010) Preventing disease through healthy environments-exposure to lead: a major public health concern. WHO, Geneva

Wu K, Wang M, Li AZ, Zhao ZX, Liu T, Hao XD, Yang SJ, Jin PK (2021) The enhanced As(III) removal by Fe-Mn-Cu ternary oxide via synergistic oxidation: performances and mechanisms. Chem Eng J 406:126739. https://doi.org/10.1016/j.cej.2020.126739

Xu WH, Wang J, Wang L, Sheng GP, Liu JH, Yu HQ, Huang XJ (2013) Enhanced arsenic removal from water by hierarchically porous CeO_2–ZrO_2 nanospheres: role of surface- and structure-dependent properties. J Hazard Mater 260:498–507. https://doi.org/10.1016/j.jhazmat.2013.06.010

Yin GC, Song XW, Tao L, Sarkar B, Sarmah AK, Zhang WX, Lin QT, Xiao RB, Liu QJ, Wang HL (2020) Novel Fe-Mn binary oxide-biochar as an adsorbent for removing Cd(II) from aqueous solutions. Chem Eng J 389:124465. https://doi.org/10.1016/j.cej.2020.124465

Yoon Y, Park WK, Hwang TM, Yoon DH, Yang WS, Kang JW (2016) Comparative evaluation of magnetite–graphene oxide and magnetite-reduced graphene oxide composite for As(III) and As(V) removal. J Hazard Mater 304:196–204. https://doi.org/10.1016/j.jhazmat.2015.10.053

Zhang GS, Qu JH, Liu HJ, Liu RP, Wu RC (2007) Preparation and evaluation of a novel Fe–Mn binary oxide adsorbent for effective arsenite removal. Water Res 41:1921–1928. https://doi.org/10.1016/j.watres.2007.02.009

Zhang GS, Ren ZM, Zhang XW, Chen J (2013) Nanostructured iron(III)-copper(II) binary oxide: a novel adsorbent for enhanced arsenic removal from aqueous solutions. Water Res 47(12):4022–4031. https://doi.org/10.1016/j.watres.2012.11.059

Zhang LF, Zhu TY, Liu X, Zhang WQ (2016) Simultaneous oxidation and adsorption of As(III) from water by cerium modified chitosan ultrafine nanobiosorbent. J Hazard Mater 308:1–10. https://doi.org/10.1016/j.jhazmat.2016.01.015

Zhang W, Zhang GS, Liu CH, Li J, Zheng T, Ma J, Wang L, Jiang J, Zhai XD (2018) Enhanced removal of arsenite and arsenate by a multifunctional Fe-Ti-Mn composite oxide: photooxidation, oxidation and adsorption. Water Res 147(15):264–275. https://doi.org/10.1016/j.watres.2018.10.001

Zhang Y, Dou XM, Zhao B, Yang M, Takayama T, Kato S (2010) Removal of arsenic by a granular Fe–Ce oxide adsorbent: fabrication conditions and performance. Chem Eng J 162(1):164–170. https://doi.org/10.1016/j.cej.2010.05.021

Zhang Y, Yang M, Huang X (2003) Arsenic(V) removal with a Ce(IV)-doped iron oxide adsorbent. Chemosphere 51(9):945–952. https://doi.org/10.1016/S0045-6535(02)00850-0

Zhao YG, Li JX, Zhao LP, Zhang SW, Huang YS, Wu XL, Wang XK (2014) Synthesis of amidoxime-functionalized Fe_3O_4@SiO_2 core–shell magnetic microspheres for highly efficient sorption of U(VI). Chem Eng J 235:275–283. https://doi.org/10.1016/j.cej.2013.09.034

Zheng Q, Hou JT, Hartley W, Ren L, Wang MX, Tu SX, Tan WF (2020) As(III) adsorption on Fe-Mn binary oxides: are Fe and Mn oxides synergistic or antagonistic for arsenic removal? Chem Eng J 389:124470. https://doi.org/10.1016/j.cej.2020.124470